

Detonation shock dynamics and comparisons with direct numerical simulation

Tariq D. Aslam*, and D. Scott Stewart†

December 13, 1997

Abstract

Comparisons between direct numerical simulation (DNS) of detonation and detonation shock dynamics (DSD) is made. The theory of DSD defines the motion of the detonation shock in terms of intrinsic geometry of the shock surface, in particular for condensed phase explosives the shock normal velocity, D_n , the normal acceleration, \dot{D}_n , and the total curvature, κ . In particular, the properties of three intrinsic front evolution laws are studied and compared. These are 1) Constant speed detonation (Huygens' construction), 2) Curvature dependent speed propagation ($D_n - \kappa$ relation), and 3) Curvature and speed dependent acceleration ($\dot{D}_n - D_n - \kappa$ relation). We show that it is possible to measure shock dynamics directly from simulation of the reactive Euler equations and that subsequent numerical solution of the intrinsic partial differential equation for the shock motion (e.g. a $\dot{D}_n - D_n - \kappa$ relation) reproduces the exact shock motion with high precision. Finally, a few numerical examples will be given to demonstrate the properties of these DSD intrinsic evolution laws.

*Corresponding Author, Los Alamos National Laboratory, Los Alamos, NM 87545

†University of Illinois, Urbana, IL 61801

1 Introduction

For nearly a century, the steady, one-dimensional Chapman–Jouget velocity, D_{CJ} [1], [2] has been used as a coarse prediction of experimental observations. For nearly as long, engineers have used the steady, one-dimensional results to predict the motion of unsteady, multi-dimensional detonation shock fronts. The rule that detonation front propagates at a constant speed in a direction normal to itself is equivalent to a Huygens’ construction. Although this model for detonation front motion is simple, it does not predict many aspects of multi-dimensional detonation flows. For example, detonation velocities have been observed to change by as much as 40% due to multi-dimensional effects [3]. Failure of detonation waves has also been observed experimentally. Other dynamics, such as pulsating and cellular detonations, can not be predicted by such a simple propagation rule.

Detonation shock dynamics (DSD) [4] [13] [14] [12] is an asymptotic theory whose key result is an intrinsic partial differential equation (PDE) for the dynamics of the detonation shock front. The theory of DSD defines the motion of the detonation shock in terms of intrinsic geometry of the shock surface, in particular for condensed phase explosives the shock normal velocity, D_n , the normal acceleration, \dot{D}_n , and the total curvature, κ . The engineering method of DSD does not solve the reactive Euler equations, but rather the intrinsic PDE that is associated with a particular explosive system to obtain arrival times of the detonation shock front throughout the explosive. The solution can be coupled with equation of state information to calculate shock pressures and other pertinent information. Thus it is critical to determine the intrinsic PDE whose solution can reproduce the motion of the detonation shock. It will be demonstrated that DSD can predict several aspects of unsteady multi-dimensional detonations accurately.

Once an appropriate relation for a particular explosive system is determined, the ability to predict the resulting initial-boundary-value problem for the evolution of the detonation shock front is needed. The numerical solution of the resulting intrinsic PDEs from DSD theory can be integrated analytically for problems with special geometries, such as planar, cylindrical and spherical problems, even then, it is not always possible to get a solution in closed form. Typical engineering applications involve very complicated boundaries, and the front can experience such topological changes as merging and burning out. Thus, the focus of this paper will be the numerical

solutions of these intrinsic DSD equations and verification of DSD theory by comparison with direct numerical simulation (DNS) of multi-dimensional unsteady detonation problems. We will focus on two DSD relations, the $D_n - \kappa$ relation and the $\dot{D}_n - D_n - \kappa$ relation.

2 Reactive Euler equations and direct numerical simulation

Here, comparisons between DSD theory with direct numerical simulation of detonations are made. The direct numerical simulations were carried out with a code described in [10]. The code is based on a high-order Godunov-type shock-capturing scheme. Of particular interest is the location and subsequent dynamics of the detonation front. In Section 2.1, the mathematical formulation of the detonation model used in the DNS is presented.

Since DSD theory is an approximate theory, one would like to know how well the theory predicts shock front evolution. One way of accomplishing this goal is to compare a DSD solution to an exact solution of a multi-dimensional detonation problem via a resolved numerical simulation of the reactive, compressible Euler equations.

An algorithm for solving the compressible reactive Euler equations is outlined. Then, comparisons of the dynamics of the shock front from DSD theory to the resolved DNS are made.

2.1 Reactive Euler equations

The reactive Euler equations express conservation of mass, momentum, and energy and include a reaction rate law as follows:

$$\begin{aligned}\frac{D\rho}{Dt} + \rho \vec{\nabla} \cdot \vec{u} &= 0 \quad , \\ \rho \frac{D\vec{u}}{Dt} + \vec{\nabla} p &= 0 \quad , \\ \frac{De}{Dt} + p \frac{D(1/\rho)}{Dt} &= 0 \quad , \\ \frac{D\lambda}{Dt} &= r(p, \rho, \lambda) \quad ,\end{aligned}\tag{1}$$

For purpose of illustration, the ideal equation of state (EOS) is used,

$$e = \frac{p}{\rho(\gamma - 1)} - Q\lambda \quad ,$$

where Q is the heat of detonation, λ is the reaction progress variable ($\lambda = 0$ for unreacted material, and $\lambda = 1$ for completely reacted material). The reaction rate is r .

Written in conservative form, in 2-D Cartesian coordinates, these become:

$$\begin{aligned}
(\rho)_t + (\rho u)_x + (\rho v)_y &= 0 \quad , \\
(\rho u)_t + (\rho u^2 + p)_x + (\rho uv)_y &= 0 \quad , \\
(\rho v)_t + (\rho uv)_x + (\rho v^2 + p)_y &= 0 \quad , \\
(E)_t + (uE + up)_x + (vE + vp)_y &= 0 \quad , \\
(\rho \lambda)_t + (\rho u \lambda)_x + (\rho v \lambda)_y &= \rho r(p, \rho, \lambda)
\end{aligned} \tag{2}$$

where

$$E = \rho e + \frac{\rho}{2}(u^2 + v^2)$$

is the total energy. Next, a numerical method will be presented that is used to solve the above conservation equations.

2.2 Numerical methods for simulation of the reactive Euler equations

The algorithm for numerically solving the reactive Euler equations is based on Shu and Osher's semi-discrete (method of lines) scheme [8], with Jiang and Shu's weighted essentially non-oscillatory (WENO) interpolation [9]. The details of this method, along with boundary treatment can also be found in [10]. The purpose of picking this algorithm is two-fold. First, by formulating the problem in a semi-discrete manner, spatial and temporal discretization are accomplished independent of one another. This makes the code easy to write for multi-dimensional forced problems. The second reason is that by using high-order spatial and temporal discretization, very accurate solutions are obtainable (formally at least in continuous regions of the flow).

2.3 Numerical solutions to 2-D unsteady detonations

The ideal EOS can be used as a model of condensed phase explosive provided appropriate (non-gaseous) values of the EOS parameters are chosen. Also, a rate law that reflects representative detonation time scales and reaction lengths must be given. For the studies in this paper, we take

$$r = H(p - 1\text{GPa})2.5147 \mu\text{s}^{-1}(1 - \lambda)^{\frac{1}{2}} \quad ,$$

as the rate law (H is the Heaviside function). We also use $Q = 4 \text{ mm}^2/\mu\text{s}^2$, $\gamma = 3$ and upstream conditions $p_o = 10^{-4} \text{ GPa}$, $\rho_o = 2 \text{ gm/cc}$ and $\vec{u} = 0$. These parameters give $D_{CJ} = 8 \text{ mm}/\mu\text{s}$, and a steady-state 1-D half-reaction-zone length of 1mm (with a complete reaction-zone length of roughly 4mm.) Each of the following cases were computed with 10 points in the half reaction zone (or 40 points in the complete reaction zone.) Each was also given the same initial conditions, a (numerically) steady CJ detonation traveling to the right with the shock initially located at $x = 8 \text{ mm}$. The numerical steady traveling wave was computed by placing the exact ZND solution on the grid and allowing it to come to steady state numerically. All shock capturing schemes have some transient initial start-up errors associated with the smearing of the initial shock profile. Using the numerical initial condition was done for the purposes of measuring intrinsic quantities, described later in Section 3.

2.3.1 Expanding channel

The first example examines the planar detonation diffraction around a rigid 90° corner. One expects that the detonation front will decelerate as a rarefaction wave is sent through the reaction zone. Figure 1 shows this phenomenon as a Schlieren-like plot at $6\mu\text{s}$, which is a gray-scale plot of $|\vec{\nabla}\rho|$ (At time $t = 0$, the planar detonation shock is located at $x = 8\text{mm}$, in the lower ($y < 35\text{mm}$) channel). Figure 1 shows the contact discontinuity (above the vortex at the corner) associated with a change in the temperature of the shocked material near the corner which also corresponds to a lower shock pressure, and thus a detonation front traveling below the CJ speed. Also, notice that it takes a finite time for the shock front (near the bottom wall) to sense the effects of the rarefaction wave. This is clearly shown in the Schlieren plot.

2.3.2 Converging channel

This second example focuses on the converging dynamics of detonations. Here, a planar-CJ detonation encounters a rigid 20° ramp. The detonation shock initially forms a Mach reflection which slowly changes to a weaker compressive wave. Now, the front speed is increased above the CJ value in the Mach-stem area. Figure 2 shows the Schlieren gray-scale image at $7\mu\text{s}$ (At time $t = 0$, the planar detonation shock is located at $x = 8\text{mm}$, in the channel). The reflected shock wave can be seen clearly, but note that the Mach stem is curved due to reaction-zone effects.

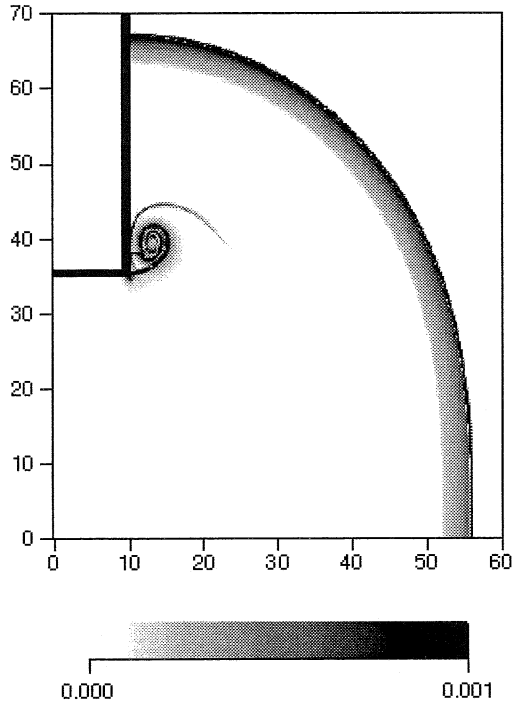


Figure 1: Schlieren-like gray-scale plot of $|\vec{\nabla}\rho| - [gm/mm^4]$ at $6\mu s$, as computed by the fifth-order WENO scheme.

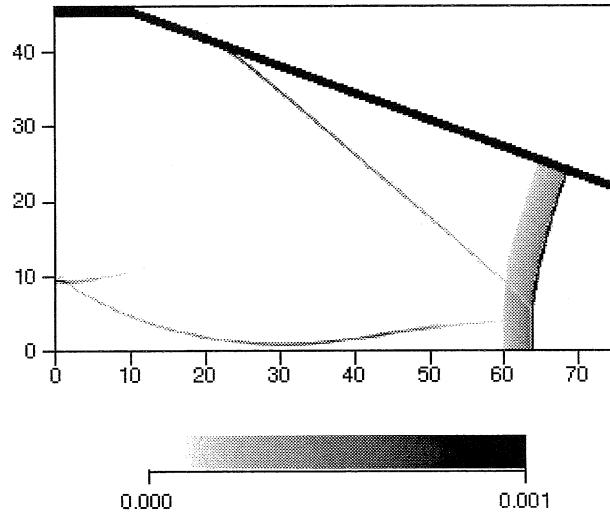


Figure 2: Schlieren-like gray-scale plot of $|\vec{\nabla}\rho| - [gm/mm^4]$ at $7\mu s$, as computed by the fifth-order WENO scheme.

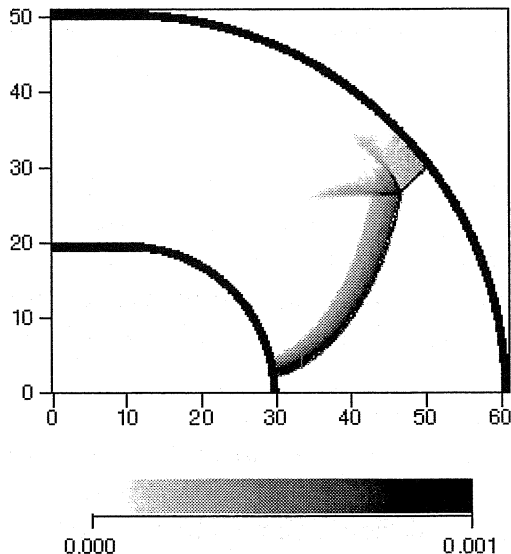


Figure 3: Schlieren-like gray-scale plot of $|\vec{\nabla}\rho| - [gm/mm^4]$ at $5\mu s$, as computed by the fifth-order WENO scheme.

2.3.3 Circular arc

The final example combines both converging and diverging aspects of detonation propagation. An initially planar detonation in a channel encounters a circular bend. The bend has an inner radius of 20mm and an outer radius of 50mm. See Figure 3. A rarefaction wave is initially generated at the inner bend, while a compressive wave is generated from the outer bend. These each influence the shape of the propagating detonation front. At about $3\mu s$ after the detonation front encounters the bend, the compressive wave and rarefaction wave collide; eventually the front becomes kinked and forms a Mach-like reflection as shown in Figure 3.

3 Measuring intrinsic properties of the detonation shock front

One way of comparing DSD with a DNS is to simply look at the motion of the shock fronts generated by both solutions. This will be the approach in this work. Another method would be to suppose there exists an intrinsic relation that governs a detonation shock front, and try to measure this relation directly from a DNS.

As stated previously, one can directly measure the dynamics of the detonation front by solving the compressible, reactive Euler equations with a

DNS. Unfortunately, intrinsic shock-front information like the detonation shock speed, curvature of the shock front, etc. are not directly available from a DNS. But, since the fluid under goes a very strong shock (the Mach number of the shock is about 650), for this detonation model, the density jump at the shock is roughly a constant. So the detonation front may be approximated as the locus of positions of the first occurrence of an intermediate density (3gm/cc was used in these computations), between the undisturbed density (2gm/cc) and the shocked density (4gm/cc). And for problems with quiescent upstream conditions, the detonation shock front will pass a fixed Eulerian point at most only once.

Thus, it is possible to create a DNS burn table by sweeping over the computational grid and searching for grid points where the quantity $(\rho - 3\text{gm/cc})$ changes sign from one time level to the next. The first such occurrence will be when the shock passes over that fixed Eulerian point. Then, linear interpolation in time is used to get an accurate estimate of the burn time, $t_b^{\text{DNS}}(x, y)$. Once we have this DNS burn table, important quantities such as shock speed, curvature, etc. may be found. For example, the shock speed is given by $D_n = 1/|\vec{\nabla} t_b|$. The front locations are given simply as contours of $t_b^{\text{DNS}}(x, y)$. The contours of the DNS burn times and instantaneous detonation velocities for the three previous examples are shown in Section 5. Next, we discuss the various functional forms of the intrinsic PDE's.

4 Intrinsic partial differential equations from detonation shock dynamics

4.1 Huygens' Construction

The Huygens' construction assumes the detonation normal velocity is equal to the Chapman-Jouget velocity, i.e. $D_n = D_{CJ} = 8\text{mm}/\mu\text{s}$. Numerically, this is solved using the level set algorithm presented in [5] and [6]. In particular, the level set of a field function, ψ , is used to describe the motion of the detonation shock, and the evolution of ψ is given by the level set equation

$$\frac{\partial \psi}{\partial t} + D_{CJ} |\vec{\nabla} \psi| = 0. \quad (3)$$

4.2 $D_n - \kappa$ relation

A $D_n - \kappa$ relation gives parabolic front evolution, see [7]. Disturbances to the shock front diffuse across the front via parabolic evolution. For this ideal model, DSD theory [4] gives a linear $D_n(\kappa)$ relation $D_n = 8\text{mm}/\mu\text{s} -$

$66.8\text{mm}^2/\mu\text{s } \kappa$. For comparison to previous results in [6], we use a $D_n(\kappa)$ shown in Figure 4. Since the $D_n - \kappa$ curve is generated numerically, a polynomial fit is used in these computations. For $\kappa < 0$, the $D_n - \kappa$ relation used is a linear extrapolation from $\kappa > 0$, which gives $D_n = 8\text{mm}/\mu\text{s} - 66.8\text{mm}^2/\mu\text{s } \kappa$. The motion of the detonation shock is solved numerically with the level set algorithm presented in [5] and [6]. For this type of intrinsic relation, the following level set equation is solved,

$$\frac{\partial \psi}{\partial t} + D_n(\kappa)|\vec{\nabla} \psi| = 0, \quad (4)$$

where $D_n(\kappa)$ is shown in Figure 4.

4.3 $\dot{D}_n - D_n - \kappa$ relation

Unlike the $D_n - \kappa$ relation, a $\dot{D}_n - D_n - \kappa$ relation is hyperbolic under certain conditions, see the discussion in [7]. In particular, disturbances at the shock front will propagate at finite speeds along the shock front. The square root of the ratio of the coefficients between κ and \dot{D}_n determines this transverse signaling speed, see [7].

The full reactive Euler equations will also have disturbances travel at finite speeds along a shock front. Essentially, an infinitesimal disturbance will travel outwards along the wavefront normal at a speed equal to the local sound speed plus it will be advected with the local particle speed. A simple analysis of inert strong shock states (for ideal EOS) shows that a disturbance will travel at a speed $[(\gamma - 1)/(\gamma + 1)]^{1/2} D_n$, see pg. 249 of [11]. A more detailed analysis including the reaction zone effects has been carried out to see if the transverse signaling speed will be changed by a reaction zone structure. It turns out that a signal will travel transverse to the shock at a speed equal to the maximum value of $(c^2 - u^2)^{1/2}$ within the reaction zone (here, c is the local sound speed, and u is the local particle velocity relative to the shock). For $\gamma > 2$, this value is maximum at the shock, and thus disturbances will travel at a speed equal to the inert case, $[(\gamma - 1)/(\gamma + 1)]^{1/2} D_n$. For $\gamma < 2$, there is an interior point in the reaction zone which has a maximum value of $(c^2 - u^2)^{1/2}$. In this case, the disturbance will travel faster than the inert shock case. For $\gamma = 3$, the transverse propagation speed of a disturbance will travel at $D_n/2^{1/2}$.

DSD theory derives a $\dot{D}_n - D_n - \kappa$ relation which can not be written as $\dot{D}_n(D_n, \kappa)$, since \dot{D}_n is not defined for certain regions of (D_n, κ) space, and is multivalued for others [12]. So, instead a functional form of the $\dot{D}_n - D_n - \kappa$ relation was chosen to give the steady $D_n(\kappa)$ relation of Section 4.2 when $\dot{D}_n = 0$. The rest of the $\dot{D}_n - D_n - \kappa$ function was determined by setting the

transverse signaling speed of the $\dot{D}_n - D_n - \kappa$ relation to be that of the full reactive Euler equations. This gives the following $\dot{D}_n - D_n - \kappa$ relation:

$$\dot{D}_n(D_n, \kappa) = -\frac{1}{2}D_n^2\kappa + \beta(D_n)$$

where

$$\beta(D_n) = \begin{cases} 3.832(\ln(8) - \ln(D_n))(1 + .145(8 - D_n)^{1/4}), & \text{if } D_n < 8 \\ .007485D_n^2(8 - D_n), & \text{if } D_n \geq 8. \end{cases}$$

Note that this $\dot{D}_n - D_n - \kappa$ relation was not derived, but rather empirically determined. A contour plot of the above relation is shown in Figure 5. Notice that the contour $\dot{D}_n = 0$ gives essentially the steady $D_n - \kappa$ relation of Figure 4. Since the normal acceleration of the front is needed, the level set PDE will need to be modified to reflect this type of relation. The equation for the level-set function, ψ , is basically unchanged from (4), except that the velocity, D_n , is now a variable. The level-set equation becomes

$$\frac{\partial \psi}{\partial t} + D_n |\vec{\nabla} \psi| = 0, \quad (5)$$

and the total derivative of D_n is given as

$$\frac{D(D_n)}{Dt} = \frac{\partial D_n}{\partial t} + D_n \hat{n} \cdot \vec{\nabla} D_n = \dot{D}_n(D_n, \kappa), \quad (6)$$

where \hat{n} is the shock front normal, $\hat{n} = \vec{\nabla} \psi / |\vec{\nabla} \psi|$. These equations form a coupled set of nonlinear PDEs for the evolution of the level-set function and its normal velocity. These equations (5) and (6) are solved in the following conservative form:

$$\begin{aligned} (u)_t + (D_n(u^2 + v^2)^{1/2})_x &= 0, \\ (v)_t + (D_n(u^2 + v^2)^{1/2})_y &= 0, \\ (D_n)_t + \left(\frac{D_n^2 u}{2(u^2 + v^2)^{1/2}}\right)_x + \left(\frac{D_n^2 v}{2(u^2 + v^2)^{1/2}}\right)_y &= \beta(D_n), \end{aligned} \quad (7)$$

where $u = \psi_x$, and $v = \psi_y$.

These equations are solved numerically using a Lax-Freidrichs algorithm with second order MinMod interpolation described in [10]. Next, the detonation front dynamics generated from the DNS are compared with those from the three intrinsic relationships.

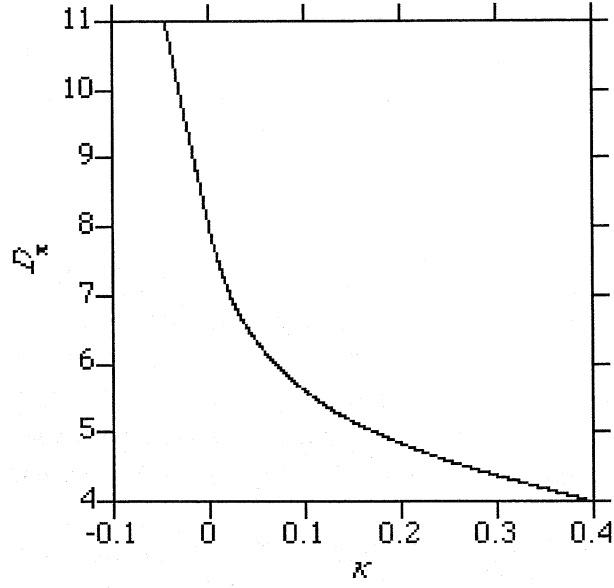


Figure 4: $D_n(\kappa)$ law for ideal equation of state model.

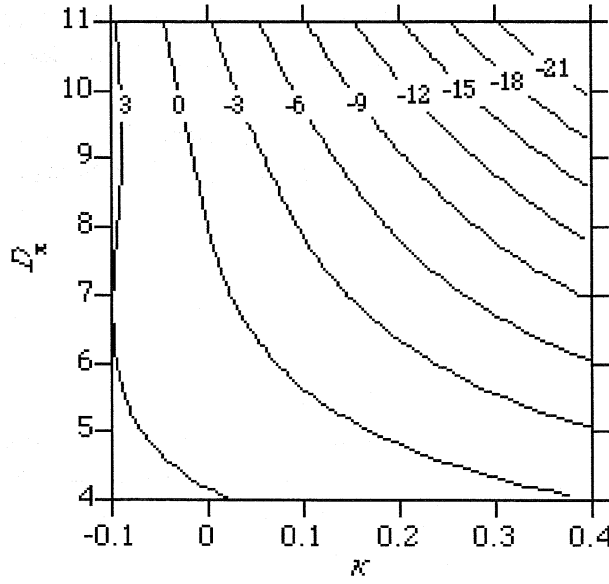


Figure 5: $\dot{D}_n - D_n - \kappa$ relation for ideal equation of state model.

5 Examples and comparisons

Here, comparisons between direct numerical simulation of detonation, and level-set solutions to three intrinsic PDEs are made. The three intrinsic relations are: the Huygens' construction, a $D_n - \kappa$ relation and a $\dot{D}_n - D_n - \kappa$ relation.

5.1 Expanding channel

The measuring technique described in Section 3 is used to calculate the front locations and Eulerian records of the detonation velocity, D_n , from the DNS for the expanding channel problem. These records are displayed in Figure 6. The detonation velocity is clearly seen to decrease by roughly 50% from the D_{CJ} value of $8\text{mm}/\mu\text{s}$. Also, notice that the signaling speed is clearly evident in the simulation, and matches the correct speed given from acoustic theory [11].

The Huygens' solution is given in Figure 7. The dashed lines represent the fronts from the Huygens' solution, while the DNS fronts from Figure 6 are given as solid lines for comparison. Notice that there is a large discrepancy in the shapes and velocities of the fronts.

The $D_n - \kappa$ solution is given in Figure 8. The detonation front slows as the front goes around the corner. Also, since the underlying PDE is parabolic, the entire front instantaneously senses disturbances at the front, as seen by the gray-scale plot of the normal velocity. Although this is not physically correct, the dynamics of a $D_n - \kappa$ do predict velocity deficits, which were seen in the DNS.

The $\dot{D}_n - D_n - \kappa$ solution is given in Figure 9. Notice that the disturbances propagate at a finite speed from the corner, as predicted in Section 4.3. Notice also that for this problem the shapes and resulting detonation velocities compare well with the DNS.

5.2 Converging channel

The measuring technique described in Section 3 is again used to calculate the front locations and Eulerian records of the detonation velocity, D_n , from the DNS for the converging channel problem. These records are displayed in Figure 10. The detonation velocity is clearly seen to increase to about $9.5\text{mm}/\mu\text{s}$ from the CJ value of $8\text{mm}/\mu\text{s}$. Also, notice that the disturbance from the wedge travels at a finite speed into the steady one-dimensional detonation region.

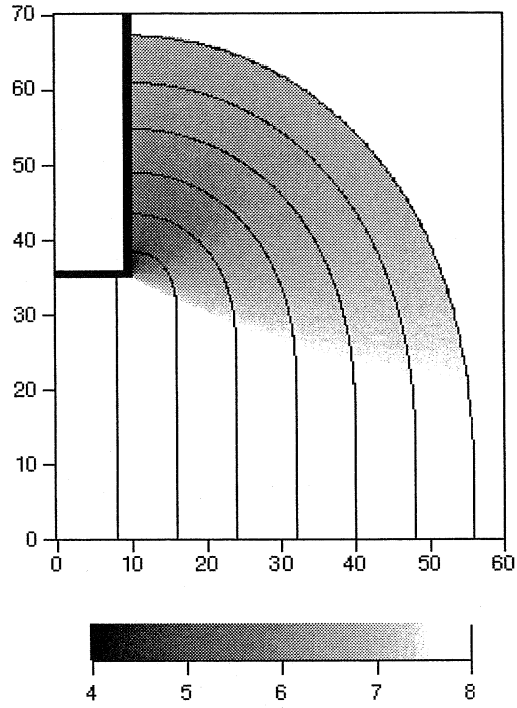


Figure 6: Fronts at intervals of $1\mu s$ are shown as solid lines, and the detonation normal velocities $[mm/\mu s]$ calculated from the DNS are given as the gray scale.

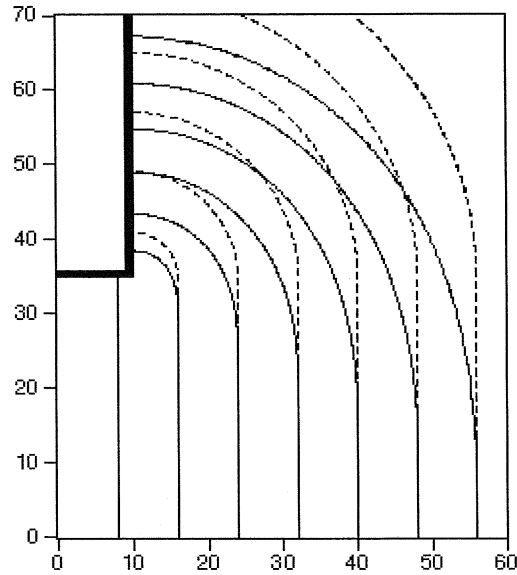


Figure 7: Fronts at intervals of $1\mu s$ are shown as solid lines from the DNS, and as dotted lines from the Huygens' solution.

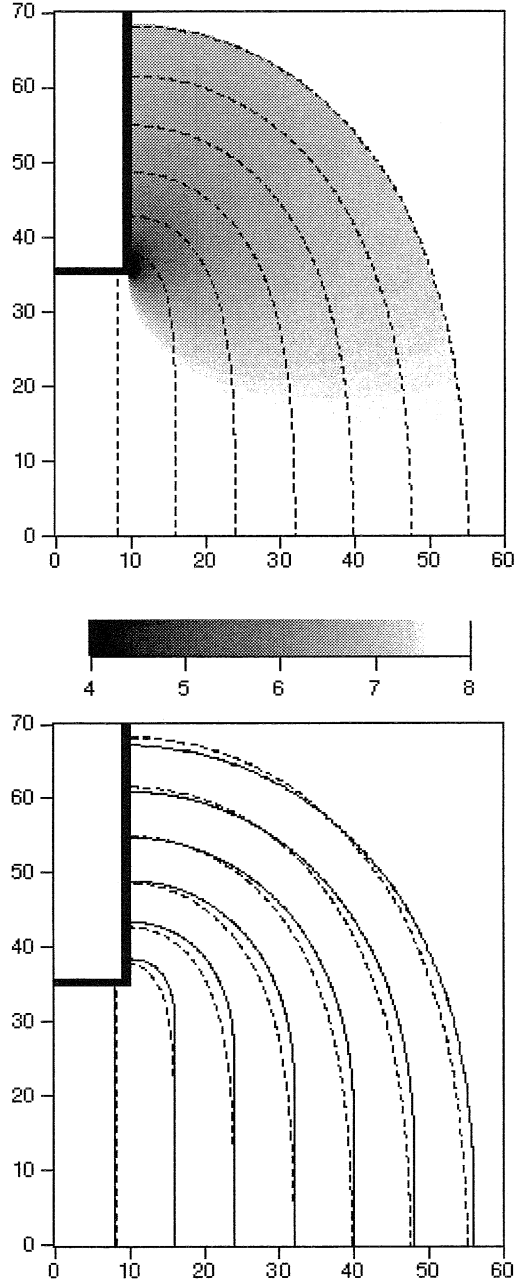


Figure 8: The top figure shows the fronts at intervals of $1\mu s$, and detonation velocities $[\text{mm}/\mu s]$ as calculated from the level-set $D_n - \kappa$ solution. Fronts are shown as solid lines from the DNS, and as dotted lines from the $D_n - \kappa$ solution in the bottom figure.

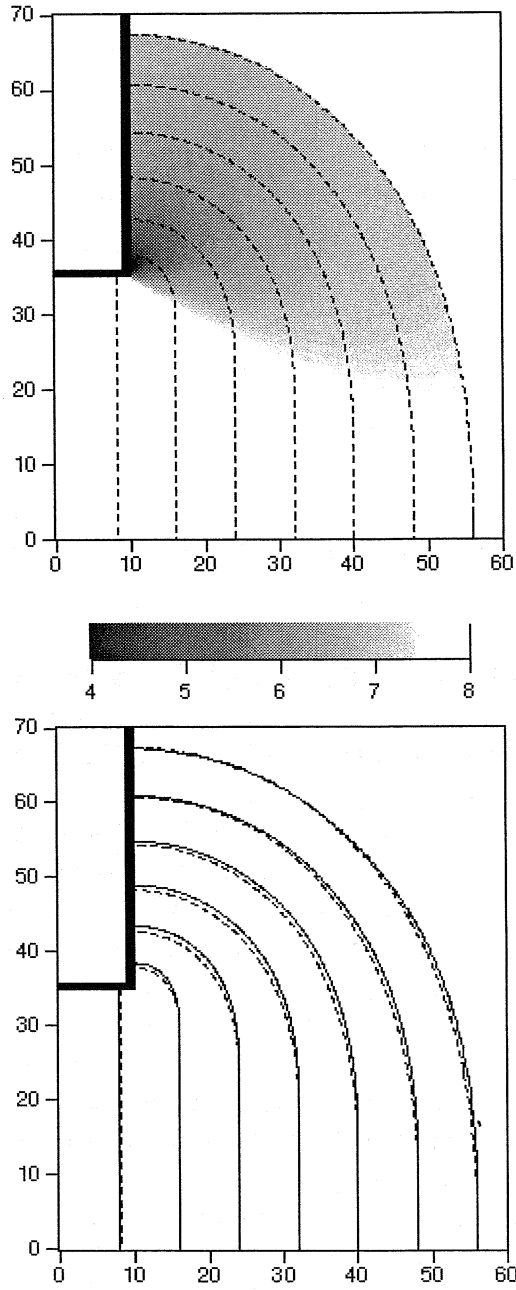


Figure 9: The top figure shows the fronts at intervals of $1\mu s$, and detonation velocities $[\text{mm}/\mu s]$ as calculated from the level-set $\dot{D}_n - D_n - \kappa$ solution. Fronts are shown as solid lines from the DNS, and as dotted lines from the $\dot{D}_n - D_n - \kappa$ solution in the bottom figure.

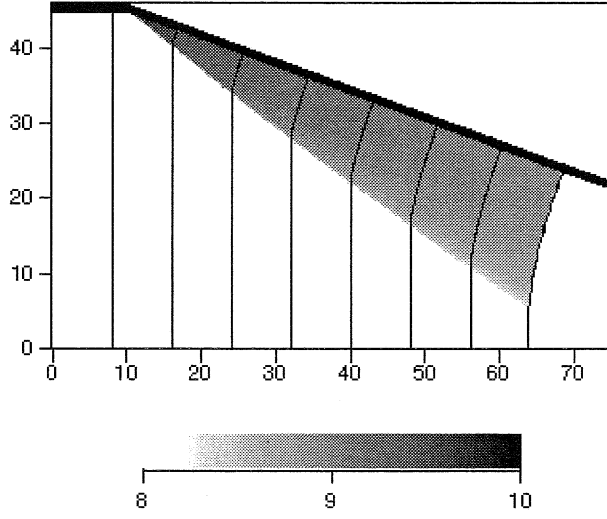


Figure 10: Fronts at intervals of $1\mu s$ are shown as solid lines, and the detonation normal velocities $[mm/\mu s]$ calculated from the DNS are given as the gray scale.

The Huygens' solution is given in Figure 11. The dashed lines represent the fronts from the Huygens' solution, while the DNS fronts from Figure 10 are given as solid lines for comparison. Notice that the Huygens' solution is just a flat wave solution, and no shape changes are predicted.

The $D_n - \kappa$ solution is given in Figure 12. The detonation front increases in speed as the front changes angle at the upper boundary to satisfy the reflection boundary condition. Since the underlying PDE is parabolic, the entire front instantaneously senses disturbances at the front, as seen by the gray-scale plot of the normal velocity. Again, this is not physically correct, but the $D_n - \kappa$ solution does predict a velocity increase.

The $\dot{D}_n - D_n - \kappa$ solution is given in Figure 13. Notice that the disturbances propagate at a finite speed from the ramp. Also notice that there is initially a kink in the wave front, associated with a shock-shock-like reflection from the ramp. This solution, unlike Whitham's Geometrical Shock Dynamics model for inerts, is not self-similar. The detonation velocity is actually decreasing along the ramp wall as a function of time. This is due to the $\beta(D_n)$ forcing term in the $\dot{D}_n - D_n - \kappa$ relation. Notice also that for this problem the shapes and resulting detonation velocities compare well with the DNS. Even though the acoustic transverse propagation speed is exactly the same as for the full compressible Euler equations, the triple point tracks are slightly different. This is due to the fact that the jump conditions for the intrinsic PDE are different than the Euler equations.

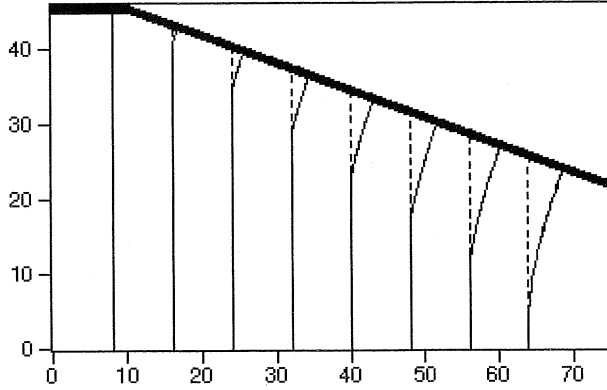


Figure 11: Fronts at intervals of $1\mu s$ are shown as solid lines from the DNS, and as dotted lines from the Huygens' solution.

5.3 Circular arc

Again the measuring technique described in Section 3 is used to calculate the front locations and Eulerian records of the detonation velocity, D_n , from the DNS for the circular arc problem. These records are displayed in Figure 14. The detonation velocity is clearly seen to increase along the outer bend, where the detonation senses a compressive wave, and is far below D_{CJ} along the inner bend, where there is a rarefaction wave, and the detonation diverges. Also, notice that the disturbance from the edges can be seen to travel at a finite speed into the steady one-dimensional detonation region.

The Huygens' solution is given in Figure 15. The dashed lines represent the fronts from the Huygens' solution, while the DNS fronts from Figure 14 are given as solid lines for comparison. Notice that the Huygens' solution predicts a flat wave along the top of the circular arc, and diffracts around the inner radius of the arc without any decrease in speed. Notice that the general shapes and locations are quite different than the DNS.

The $D_n - \kappa$ solution is given in Figure 16. The detonation front increases in speed along the upper boundary to satisfy the reflection boundary condition, and decreases along the inner radius. Also, the fronts become steady in a frame rotating with the arc very quickly, again this can be attributed to parabolic nature of the $D_n - \kappa$ relation. Although this relation does not predict the shapes very well, the fronts seem to be on average in roughly the right locations.

The $\dot{D}_n - D_n - \kappa$ solution is given in Figure 17. Notice that the disturbances propagate at a finite speed from the inner and outer bends. Also notice that there is a kink that eventually forms, when the compressive wave from the outer radius breaks and forms a shock-shock interaction. Notice

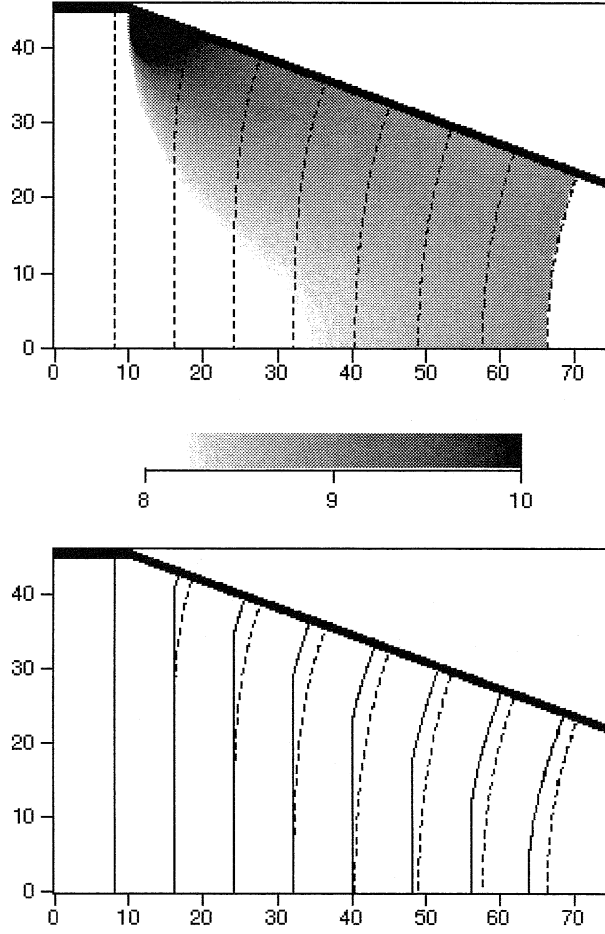


Figure 12: The top figure shows the fronts at intervals of $1\mu s$, and detonation velocities $[\text{mm}/\mu s]$ as calculated from the level-set $D_n - \kappa$ solution. Fronts are shown as solid lines from the DNS, and as dotted lines from the $D_n - \kappa$ solution in the bottom figure.

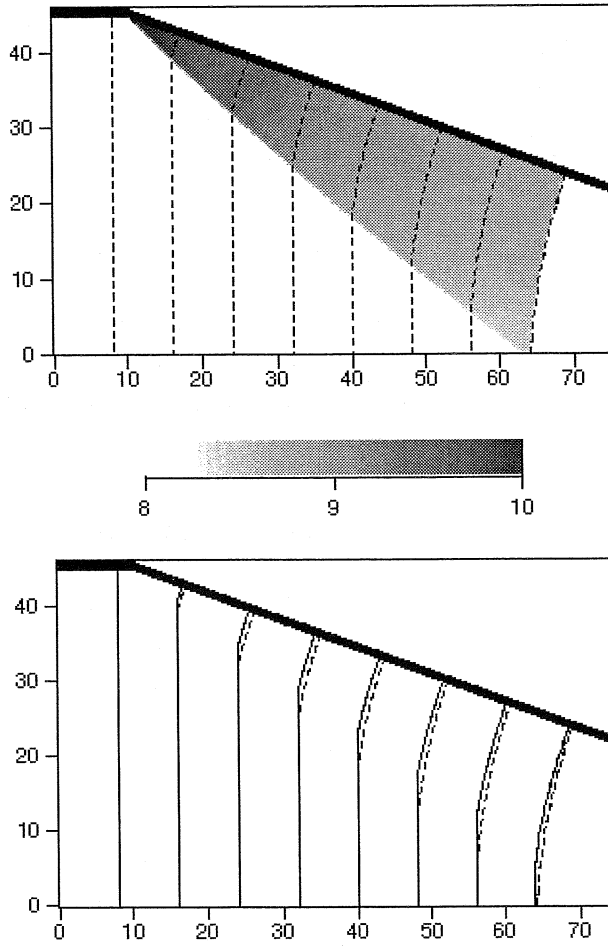


Figure 13: The top figure shows the fronts at intervals of $1\mu s$, and detonation velocities $[\text{mm}/\mu s]$ as calculated from the level-set $\dot{D}_n - D_n - \kappa$ solution. Fronts are shown as solid lines from the DNS, and as dotted lines from the $\dot{D}_n - D_n - \kappa$ solution in the bottom figure.

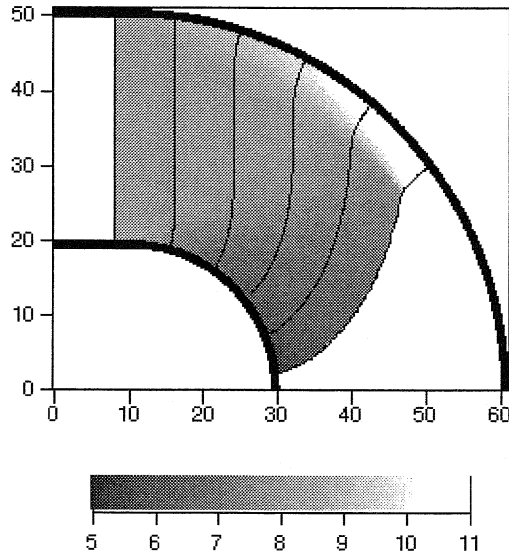


Figure 14: Fronts at intervals of $1 \mu s$ are shown as solid lines, and the detonation normal velocities [mm/ μs] calculated from the DNS are given as the gray scale.

also that for this problem the shapes and resulting detonation velocities compare well with the DNS.

Notice also that these three problems are very difficult tests, since the velocities vary far from D_{CJ} , and the curvatures, and time dependence are relatively large.

6 Conclusions

From the examples given here, it seems clear that the ability of a $\dot{D}_n - D_n - \kappa$ relation does an excellent job of reproducing the front evolution of a resolved DNS. It alleviates some of the short comings of a $D_n - \kappa$ relation. In particular, since a $\dot{D}_n - D_n - \kappa$ relation is hyperbolic, and signaling speeds are similar to the full reactive Euler equations, the range of influence of disturbances are predicted better than a $D_n - \kappa$ relation.

Acknowledgments

T. D. Aslam and D. S. Stewart have been supported by the United States Air Force (USAF), Wright Laboratory, Armament Directorate, Eglin Air Force Base, F08630-95-1-0004. Tariq Aslam has also been supported by the U.S. Department of Energy.

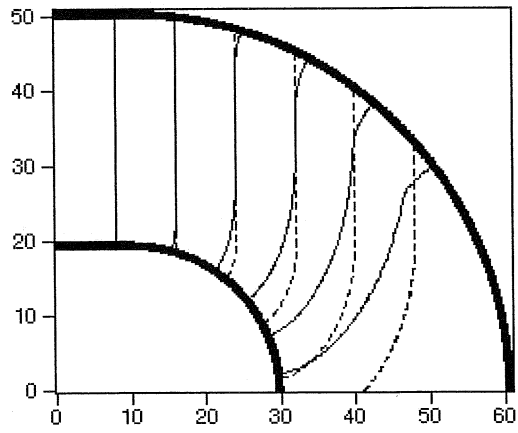


Figure 15: Fronts at intervals of $1 \mu\text{s}$ are shown as solid lines from the DNS, and as dotted lines from the Huygens' solution.

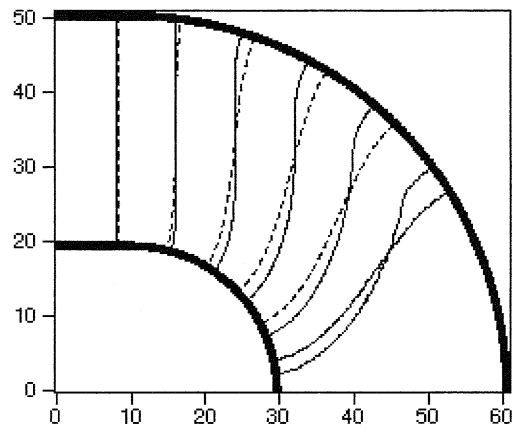
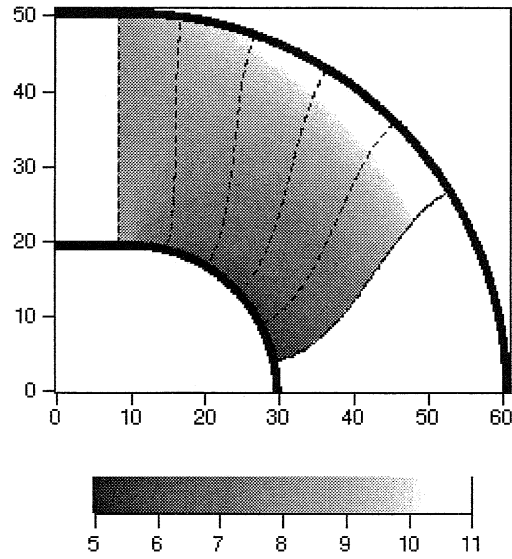


Figure 16: The top figure shows the fronts at intervals of $1 \mu s$, and detonation velocities $[\text{mm}/\mu s]$ as calculated from the level-set $D_n - \kappa$ solution. Fronts are shown as solid lines from the DNS, and as dotted lines from the $D_n - \kappa$ solution in the bottom figure.

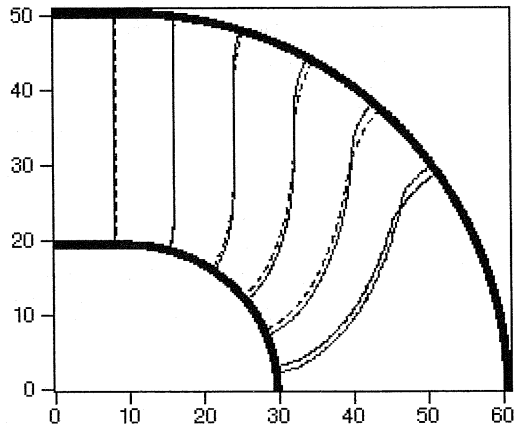
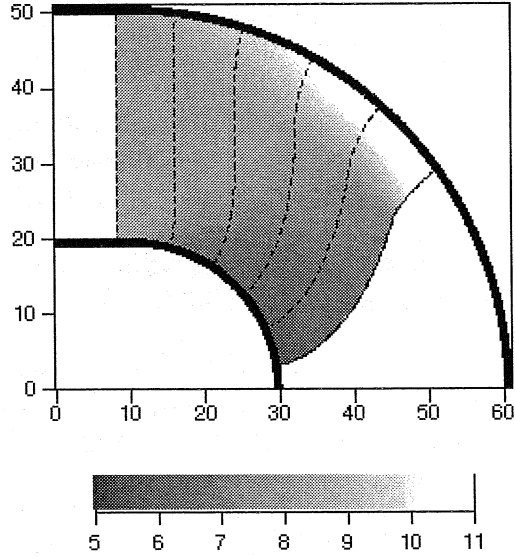


Figure 17: The top figure shows the fronts at intervals of $1 \mu s$, and detonation velocities $[\text{mm}/\mu s]$ as calculated from the level-set $\dot{D}_n - D_n - \kappa$ solution. Fronts are shown as solid lines from the DNS, and as dotted lines from the $\dot{D}_n - D_n - \kappa$ solution in the bottom figure.

References

- [1] Chapman, D. L., "On the rate of explosion in gases," *Philosophical Magazine*, 47, 90-104 (1899).
- [2] Jouguet, E., "On the propagation of chemical reactions in gases," *Journal de Mathematiques Pures et Appliquees*, 1, 347-425 and 2, 5-85 (1906).
- [3] Wood, W. W., and Kirkwood, J. G., "Diameter effect in condensed explosives. The relation between velocity and radius of curvature in the detonation wave," *Journal of Chemical Physics*, 22, 1920-1924 (1954).
- [4] Stewart, D. S. and Bdzil, J. B., "The shock dynamics of stable multidimensional detonation," *Combustion and Flame*, 72, 311-323 (1988).
- [5] Osher, Stanley and Sethian, James A., "Fronts Propagating with Curvature- Dependent Speed: Algorithms Based on Hamilton-Jacobi Formulations," *Journal of Computational Physics*, 79, 12-49 (1988).
- [6] Aslam, Tariq D., Bdzil, John B., and Stewart, D. Scott, "Level Set Methods Applied to Modeling Detonation Shock Dynamics," *Journal of Computational Physics*, 126, 390-409 (1996).
- [7] Aslam, Tariq D., "Investigations on Detonation Shock Dynamics," PhD Thesis, University of Illinois at Urbana-Champaign, (1996).
- [8] Shu, Chi-Wang and Osher, Stanley, "Efficient Implementation of Essentially Non-oscillatory Shock-Capturing Schemes II," *Journal of Computational Physics*, 83, 32-78 (1989).
- [9] Jiang, Guang-Shan and Shu, Chi-Wang, "Efficient Implementation of Weighted ENO Schemes," *Journal of Computational Physics*, 126, 202-228, (1996).
- [10] Xu, Shaojie, Aslam, Tariq, and Stewart, D. Scott, "High Resolution Numerical Simulation of Ideal and Non-ideal Compressible Reacting Flows with Embedded Internal Boundaries," *Combustion Theory and Modelling*, Vol 1, Nu 1, 113-142 (1997).
- [11] Whitham, G. B., *Linear and Nonlinear Waves*, Wiley (New York) (1974).
- [12] Yao, Jin and Stewart, D. Scott, "On the dynamics of multi-dimensional detonation," *Journal of Fluid Mechanics*, 309, 225-275 (1996)

- [13] Bdzil, J. B. and Stewart, D. S., "Modeling Two-Dimensional Detonation with Detonation Shock Dynamics," *Phys. Fluids A*, 1,1261-1267 (1989).
- [14] Stewart, D. S., and Bdzil, J. B., "A lecture on detonation shock dynamics," in *Mathematical Modeling in Combustion Science, Lecture Notes in Physics*, 299, 17-30, Springer-Verlag (New York) (1988).

List of Recent TAM Reports

No.	Authors	Title	Date
793	Harris, J. G.	Modeling scanned acoustic imaging of defects at solid interfaces—Chapter in <i>IMA Workshop on Inverse Problems in Wave Propagation</i> , G. Chevant, G. Papanicolaou, P. Sacks and W. E. Symes, eds. New York: Springer-Verlag, 237–258 (1996)	May 1995
794	Sottos, N. R., J. M. Ockers, and M. J. Swindeman	Thermoelastic properties of plain weave composites for circuit board applications— <i>ASME Journal of Electronic Packaging</i> , in press (1998)	May 1995
795	Aref, H., and M. A. Stremmer	On the motion of three point vortices in a periodic strip— <i>Journal of Fluid Mechanics</i> 314, 1–25 (1996)	June 1995
796	Barenblatt, G. I., and N. Goldenfeld	Does fully-developed turbulence exist? Reynolds number independence versus asymptotic covariance— <i>Physics of Fluids</i> 7, 3078–3082 (1995)	June 1995
797	Aslam, T. D., J. B. Bdzil, and D. S. Stewart	Level set methods applied to modeling detonation shock dynamics— <i>Journal of Computational Physics</i> 126, 390–409 (1996)	June 1995
798	Nimmagadda, P. B. R., and P. Sofronis	The effect of interface slip and diffusion on the creep strength of fiber and particulate composite materials—Proceedings of the ASME Applied Mechanics Division 213, 125–143 (1995)	July 1995
799	Hsia, K. J., T.-L. Zhang, and D. F. Socie	Effect of crack surface morphology on the fracture behavior under mixed mode loading— <i>Fatigue and Fracture Mechanics</i> 27, 152–174 (1996)	July 1995
800	Adrian, R. J.	Stochastic estimation of the structure of turbulent fields—In <i>Eddy Structure Identification</i> , J. P. Bonnet, ed. Berlin: Springer, 145–196 (1996)	Aug. 1995
801	Riahi, D. N.	Perturbation analysis and modeling for stratified turbulence	Aug. 1995
802	Thoroddsen, S. T.	Conditional sampling of dissipation in high Reynolds number turbulence— <i>Physics of Fluids</i> 8, 1333–1335 (1996)	Aug. 1995
803	Riahi, D. N.	On the structure of an unsteady convecting mushy layer— <i>Acta Mechanica</i> , 127, 83–96 (1998)	Aug. 1995
804	Meleshko, V. V.	Equilibrium of an elastic rectangle: The Mathieu–Inglis–Pickett solution revisited— <i>Journal of Elasticity</i> 40, 207–238 (1995)	Aug. 1995
805	Jonnalagadda, K., G. E. Kline, and N. R. Sottos	Local displacements and load transfer in shape memory alloy composites— <i>Experimental Mechanics</i> 37, 82–90 (1997)	Aug. 1995
806	Nimmagadda, P. B. R., and P. Sofronis	On the calculation of the matrix–reinforcement interface diffusion coefficient in composite materials at high temperatures— <i>Acta Metallurgica et Materialia</i> 44, 2711–2716 (1996)	Aug. 1995
807	Carlson, D. E., and D. A. Tortorelli	On hyperelasticity with internal constraints— <i>Journal of Elasticity</i> 42, 91–98 (1996)	Aug. 1995
808	Sayre, T. L., and D. N. Riahi	Oscillatory instabilities of the liquid and mushy layers during solidification of alloys under rotational constraint— <i>Acta Mechanica</i> 121, 143–152 (1997)	Sept. 1995
809	Xin, Y.-B., and K. J. Hsia	Simulation of the brittle–ductile transition in silicon single crystals using dislocation mechanics— <i>Acta Metallurgica et Materialia</i> 45, 1747–1759 (1997)	Oct. 1995
810	Ulysse, P., and R. E. Johnson	A plane-strain upper-bound analysis of unsymmetrical single-hole and multi-hole extrusion processes	Oct. 1995
811	Fried, E.	Continua described by a microstructural field— <i>Zeitschrift für angewandte Mathematik und Physik</i> 47, 168–175 (1996)	Nov. 1995
812	Mittal, R., and S. Balachandar	Autogeneration of three-dimensional vortical structures in the near wake of a circular cylinder	Nov. 1995
813	Segev, R., E. Fried, and G. de Botton	Force theory for multiphase bodies— <i>Journal of Geometry and Physics</i> 20, 371–392 (1996)	Dec. 1995
814	Weaver, R. L.	The effect of an undamped finite-degree-of-freedom “fuzzy” substructure: Numerical solutions and theoretical discussion— <i>Journal of the Acoustical Society of America</i> 100, 3159–3164 (1996)	Jan. 1996

List of Recent TAM Reports (cont'd)

No.	Authors	Title	Date
815	Haber, R. B., C. S. Jog, and M. P. Bendsøe	A new approach to variable-topology shape design using a constraint on perimeter— <i>Structural Optimization</i> 11 , 1–12 (1996)	Feb. 1996
816	Xu, Z.-Q., and K. J. Hsia	A numerical solution of a surface crack under cyclic hydraulic pressure loading— <i>ASME Journal of Tribology</i> 119 , 637–645 (1997)	Mar. 1996
817	Adrian, R. J.	Bibliography of particle velocimetry using imaging methods: 1917–1995— <i>Produced and distributed in cooperation with TSI, Inc., St. Paul, Minn.</i>	Mar. 1996
818	Fried, E., and G. Grach	An order-parameter based theory as a regularization of a sharp-interface theory for solid–solid phase transitions— <i>Archive for Rational Mechanics and Analysis</i> 138 , 355–404 (1997)	Mar. 1996
819	Vonderwell, M. P., and D. N. Riahi	Resonant instability mode triads in the compressible boundary-layer flow over a swept wing— <i>International Journal of Engineering Science</i> , in press (1997)	Mar. 1996
820	Short, M., and D. S. Stewart	Low-frequency two-dimensional linear instability of plane detonation— <i>Journal of Fluid Mechanics</i> 340 , 249–295 (1997)	Mar. 1996
821	Casagrande, A., and P. Sofronis	On the scaling laws for the consolidation of nanocrystalline powder compacts— <i>Proceedings of the IUTAM Symposium on the Mechanics of Granular and Porous Materials</i> , N. A. Fleck and A. C. F. Cocks, eds. The Netherlands: Kluwer Academic Publishers, 105–116 (1997)	Apr. 1996
822	Xu, S., and D. S. Stewart	Deflagration-to-detonation transition in porous energetic materials: A comparative model study— <i>Journal of Engineering Mathematics</i> 31 , 143–172 (1997)	Apr. 1996
823	Weaver, R. L.	Mean and mean-square responses of a prototypical master/fuzzy structure— <i>Journal of the Acoustical Society of America</i> 101 , 1441–1449 (1997)	Apr. 1996
824	Fried, E.	Correspondence between a phase-field theory and a sharp-interface theory for crystal growth— <i>Continuum Mechanics and Thermodynamics</i> 9 , 33–60 (1997)	Apr. 1996
825	Students in TAM 293–294	Thirty-third student symposium on engineering mechanics, J. W. Phillips, coordinator: Selected senior projects by W. J. Fortino II, A. A. Mordock, and M. R. Sawicki	May 1995
826	Riahi, D. N.	Effects of roughness on nonlinear stationary vortices in rotating disk flows— <i>Mathematical and Computer Modeling</i> 25 , 71–82 (1997)	June 1996
827	Riahi, D. N.	Nonlinear instabilities of shear flows over rough walls	June 1996
828	Weaver, R. L.	Multiple scattering theory for a plate with sprung masses, mean responses— <i>Journal of the Acoustical Society of America</i> 101 , 3466–3414 (1997)	July 1996
829	Moser, R. D., M. M. Rogers, and D. W. Ewing	Self-similarity of time-evolving plane wakes <i>Journal of Fluid Mechanics</i> , in press (1998)	July 1996
830	Lufrano, J. M., and P. Sofronis	Enhanced hydrogen concentrations ahead of rounded notches and cracks: Competition between plastic strain and hydrostatic stress— <i>Acta Metallurgica et Materialia</i> , in press (1998)	July 1996
831	Riahi, D. N.	Effects of surface corrugation on primary instability modes in wall-bounded shear flows	Aug. 1996
832	Bechel, V. T., and N. R. Sottos	Application of debond length measurements to examine the mechanics of fiber pushout	Aug. 1996
833	Riahi, D. N.	Effect of centrifugal and Coriolis forces on chimney convection during alloy solidification— <i>Journal of Crystal Growth</i> 179 , 287–296 (1997)	Sept. 1996
834	Cermelli, P., and E. Fried	The influence of inertia on configurational forces in a deformable solid— <i>Proceedings of the Royal Society of London A</i> 453 , 1915–1927 (1997)	Oct. 1996
835	Riahi, D. N.	On the stability of shear flows with combined temporal and spatial imperfections	Oct. 1996

List of Recent TAM Reports (cont'd)

No.	Authors	Title	Date
836	Carranza, F. L., B. Fang, and R. B. Haber	An adaptive space-time finite element model for oxidation-driven fracture, <i>Computer Methods in Applied Mechanics and Engineering</i> , in press (1997)	Nov. 1996
837	Carranza, F. L., B. Fang, and R. B. Haber	A moving cohesive interface model for fracture in creeping materials, <i>Computational Mechanics</i> 19, 517-521 (1997)	Nov. 1996
838	Balachandar, S., R. Mittal, and F. M. Najjar	Properties of the mean wake recirculation region in two-dimensional bluff body wakes— <i>Journal of Fluid Mechanics</i> , in press (1997)	Dec. 1996
839	Ti, B. W., W. D. O'Brien, Jr., and J. G. Harris	Measurements of coupled Rayleigh wave propagation in an elastic plate— <i>Journal of the Acoustical Society of America</i> 102, 1528-1531	Dec. 1996
840	Phillips, W. R. C.	On finite-amplitude rotational waves in viscous shear flows— <i>Studies in Applied Mathematics</i> 100, in press (1998)	Jan. 1997
841	Riahi, D. N.	Direct resonance analysis and modeling for a turbulent boundary layer over a corrugated surface— <i>Acta Mechanica</i> , in press (1998)	Jan. 1997
842	Liu, Z.-C., R. J. Adrian, C. D. Meinhart, and W. Lai	Structure of a turbulent boundary layer using a stereoscopic, large format video-PIV— <i>Developments in Laser Techniques and Fluid Mechanics</i> , 259-273 (1997)	Jan. 1997
843	Fang, B., F. L. Carranza, and R. B. Haber	An adaptive discontinuous Galerkin method for viscoplastic analysis— <i>Computer Methods in Applied Mechanics and Engineering</i> 150, 191-198 (1997)	Jan. 1997
844	Xu, S., T. D. Aslam, and D. S. Stewart	High-resolution numerical simulation of ideal and non-ideal compressible reacting flows with embedded internal boundaries— <i>Combustion Theory and Modeling</i> 1, 113-142 (1997)	Jan. 1997
845	Zhou, J., C. D. Meinhart, S. Balachandar, and R. J. Adrian	Formation of coherent hairpin packets in wall turbulence—In <i>Self-Sustaining Mechanisms in Wall Turbulence</i> , R. L. Panton, ed. Southampton, UK: Computational Mechanics Publications, 109-134 (1997)	Feb. 1997
846	Lufrano, J. M., P. Sofronis, and H. K. Birnbaum	Elastoplastically accommodated hydride formation and embrittlement— <i>Journal of Mechanics and Physics of Solids</i> , in press (1998)	Feb. 1997
847	Keane, R. D., N. Fujisawa, and R. J. Adrian	Unsteady non-penetrative thermal convection from non-uniform surfaces—In <i>Geophysical and Astrophysical Convection</i> , R. Kerr, ed. (1997)	Feb. 1997
848	Aref, H., and M. Brøns	On stagnation points and streamline topology in vortex flows	Mar. 1997
849	Asghar, S., T. Hayat, and J. G. Harris	Diffraction by a slit in an infinite porous barrier— <i>Wave Motion</i> , in press (1998)	Mar. 1997
850	Shawki, T. G., H. Aref, and J. W. Phillips	Mechanics on the Web—Proceedings of the International Conference on Engineering Education (Aug. 1997, Chicago)	Apr. 1997
851	Stewart, D. S., and J. Yao	The normal detonation shock velocity-curvature relationship for materials with non-ideal equation of state and multiple turning points— <i>Combustion and Flame</i> , in press (1998)	Apr. 1997
852	Fried, E., A. Q. Shen, and S. T. Thoroddsen	Wave patterns in a thin layer of sand within a rotating horizontal cylinder, Meeting of the APS Fluids Division (1997)	Apr. 1997
853	Boyland, P. L., H. Aref, and M. A. Stremler	Topological fluid mechanics of stirring	Apr. 1997
854	Parker, S. J., and S. Balachandar	Viscous and inviscid instabilities of flow along a streamwise corner— <i>Theoretical and Computational Fluid Dynamics</i> , in press (1997)	May 1997
855	Soloff, S. M., R. J. Adrian, and Z.-C. Liu	Distortion compensation for generalized stereoscopic particle image velocimetry— <i>Measurement Science and Technology</i> 8, 1-14 (1997)	May 1997
856	Zhou, Z., R. J. Adrian, S. Balachandar, and T. M. Kendall	Mechanisms for generating coherent packets of hairpin vortices in near-wall turbulence— <i>Journal of Fluid Mechanics</i> , in press (1997)	June 1997

List of Recent TAM Reports (cont'd)

<i>No.</i>	<i>Authors</i>	<i>Title</i>	<i>Date</i>
857	Neishtadt, A. I., D. L. Vainshtein, and A. A. Vasiliev	Chaotic advection in a cubic stokes flow— <i>Physica D</i> 111 , 227 (1997).	June 1997
858	Weaver, R. L.	Ultrasonics in an aluminum foam— <i>Ultrasonics</i> , in press (1997)	July 1997
859	Riahi, D. N.	High gravity convection in a mushy layer during alloy solidification—In <i>Nonlinear Instability, Chaos and Turbulence</i> , D. N. Riahi and L. Debnath, eds., in press (1998)	July 1997
860	Najjar, F. M., and S. Balachandar	Low-frequency unsteadiness in the wake of a normal plate, <i>Journal of Fluid Mechanics</i> , in press (1997)	Aug. 1997
861	Short, M.	A parabolic linear evolution equation for cellular detonation instability	Aug. 1997
862	Short, M., and D. S. Stewart	Cellular detonation stability—I: A normal-mode linear analysis	Sept. 1997
863	Carranza, F. L., and R. B. Haber	A numerical study of intergranular fracture and oxygen embrittlement in an elastic-viscoplastic solid— <i>Journal of the Mechanics and Physics of Solids</i> , in press (1997)	Oct. 1997
864	Sakakibara, J., and R. J. Adrian	Whole-field measurement of temperature in water using two-color laser-induced fluorescence	Oct. 1997
865	Riahi, D. N.	Effect of surface corrugation on convection in a three-dimensional finite box of fluid-saturated porous material	Oct. 1997
866	Baker, C. F., and D. N. Riahi	Three-dimensional flow instabilities during alloy solidification	Oct. 1997
867	Fried, E.	Introduction (only) to <i>The Physical and Mathematical Foundations of the Continuum Theory of Evolving Phase Interfaces</i> (book containing 14 seminal papers dedicated to Morton E. Gurtin), Berlin: Springer-Verlag, in press (1998)	Oct. 1997
868	Folguera, A., and J. G. Harris	Coupled Rayleigh surface waves in a slowly varying elastic waveguide	Oct. 1997
869	Stewart, D. S.	Detonation shock dynamics: Application for precision cutting of metal with detonation waves	Oct. 1997
870	Shrotriya, P., and N. R. Sottos	Creep and relaxation behavior of woven glass/epoxy substrates for multilayer circuit board applications	Nov. 1997
871	Riahi, D. N.	Boundary wave-vortex interaction in channel flow at high Reynolds numbers	Nov. 1997
872	George, W. K., L. Castillo, and M. Wosnik	A theory for turbulent pipe and channel flows—paper presented at <i>Disquisitiones Mechanicae</i> (Urbana, Ill., October 1996)	Nov. 1997
873	Aslam, T. D., and D. S. Stewart	Detonation shock dynamics and comparisons with direct numerical simulation	Dec. 1997